Letter

Temperature, enthalpy, and kinetics of cerium resolidification under dynamic compression

T. M. Hartsfield,[1,*] B. M. La Lone,[2,†] G. D. Stevens,[2] M. T. Beason,[1] J. K. Baldwin,[1] and W. D. Turley[2]
[1]*Los Alamos National Laboratory, Los Alamos, New Mexico 87545, USA*
[2]*Nevada National Security Site, Special Technologies Laboratory, Santa Barbara, California 93111, USA*

(Received 26 March 2023; revised 16 August 2023; accepted 7 September 2023; published 6 October 2023)

We report a method to measure the temperature and transition time of cerium resolidification after shock to the liquid phase. Coating the highly reactive metal onto an inert optical window allows a supported shock to take a pure sample through an isobaric thermodynamic trajectory as diffusion cools the sample under steady stress. We measure the temperature of the liquid-to-epsilon transformation at a range of pressures to map the melt boundary under dynamic compression. We use the transformation duration to bound transformation kinetics, constrain transformation enthalpy and entropy, and explain discrepancies in predicted Hugoniot and melt coexistence in published equation-of-state models. This technique enables exploration of dynamic phase transformation in a variety of shocked materials.

DOI: 10.1103/PhysRevB.108.L140101

Locating phase boundaries in materials under dynamic compression has been a central challenge for decades in the field of shock physics. Phase transitions under hydrostatic pressure were measured by Bridgman [1] and in subsequent work by Jayaraman [2] and others using diamond-anvil cell (DAC) compression. When Bancroft *et al.* [3] reported the $\alpha - \epsilon$ phase transition in iron under dynamic loading, it substantially validated the field of shock physics. Subsequent studies used the variation in shock or sound speed in relation to particle velocity to infer the presence of a phase change [4–8]. The recent coupling of dynamic drivers with advanced light sources [9–11] has taken the field further; x-ray diffraction (XRD) directly probes the phase of the material without appealing to theory or static measurements. However, locating a phase boundary in pressure-density (P–ρ) space is often insufficient to fully constrain a multiphase equation of state (EOS). Experimentally determining the temperature (T) of the shock state through wave speeds is impossible. Inferring T from x-ray diagnostics requires a number of assumptions about the material to determine temperature reliably and precisely; so far this has not proven feasible [12].

First-order transitions are defined by the specific volume ($v = \frac{1}{\rho}$) and entropy (S) change under isobaric or isothermal conditions, but dynamic experiments typically probe the behavior of a material along an adiabatic path with varying P and T. A means of probing the P–T path of a boundary as well as the transition enthalpy would fully constrain a first-order transition (such as melting) and provide otherwise inaccessible information necessary for the validation of the multiphase EOS. The ongoing maturation of dynamic temperature measurement via optical pyrometry has enabled attempts to correlate phase and temperature. Early pyrometry studies attempted to determine the dynamic melt boundaries of materials by systematically measuring shock temperature points across a range of shock stresses; refinements of this method have been pursued up to the present [13–18]. This requires an extensive series of experiments, each with well-understood thermal properties statistically combined to reduce measurement scatter. La Lone *et al.* [19] used stress releases from the backs of flyer impactors to measure two-dimensional $P - T$ paths through the phase space of Sn, looking for inflections and coincidences indicative of the melt boundary. This technique maps the boundary with greater fidelity in fewer experiments. However, it cannot locate boundaries that do not intersect a release isentrope. Additionally, a measurement of the volume or enthalpy change, H, at constant P is still needed to fully constrain the transition, i.e., $\frac{dP}{dT} = \frac{H}{T\Delta v}$.

Pyrometric temperature measurements of metals require measurement [18] or estimation [20] of emissivity and are necessarily performed at a radiant interface across which thermal diffusion may occur on the scale of microns within the timescale of shock-wave experiments [21]. A thorough understanding of the interface properties is needed to interpret the measured temperatures and infer T in the bulk material, far from the interface. See, for example, Grover and Urtiew [22]. The pyrometric method of attaching an opaque sample to a transparent anvil window via epoxy bond may simplify this understanding by reducing thermal conduction out of the sample, but epoxy can only be used at sufficiently low P and T.

In this work we exploit thermal equilibration of a thin film of shocked cerium (Ce) coated directly onto a lithium fluoride (LiF) window to explore a portion of its high-pressure phase diagram. Ce has a complex phase diagram containing multiple

*Present address: Sandia National Laboratories, Albuquerque, New Mexico 87185, USA; thartsf@sandia.gov
†lalonebm@nv.doe.gov

Published by the American Physical Society under the terms of the Creative Commons Attribution 4.0 International license. Further distribution of this work must maintain attribution to the author(s) and the published article's title, journal citation, and DOI.

phases, the boundaries of which have been the subject of experimental and theoretical temperature and phase studies [11,17,18,23–26]. It is a highly reactive metal, making experimental samples especially prone to surface deterioration [17,18]. This complicates the interpretation of measured interface T and its relation to the bulk shock temperature of pure Ce.

Rather than attempt to infer a temperature state far from the measurement interface, we measure the film temperature at the interface as an indication of dynamic phase change in the film, in this case resolidification of shocked-melted Ce. The impact of the thick flyer plate imparts a shock wave in the thin-film coating. After this wave transits the film and reaches the LiF, the stress local to these interfaces quickly ($<$10 ns) reverberates to a constant value determined by the impactor velocity and the shock impedances of the impactor and window. Thermal evolution occurs over tens to hundreds of nanoseconds under the nominally steady stress conditions [27] maintained by the supported shock from the impactor. Heat generated in the Ce by its relatively large volume collapse under shock compression elevates it to an initial temperature greater than those of the impactor and window at stress equilibrium. Heat within the Ce subsequently flows out of the film and into the colder impactor and LiF, taking the Ce through an isobaric phase-space trajectory. We measure temperature evolution at the Ce–LiF interface and find that at a certain temperature, the steady Ce cooling is interrupted by the flow of latent heat out of the metal as its phase changes from liquid to (ϵ phase) solid.

We performed five plate impact experiments, each with a nominally identical target consisting of a LiF [100] crystal (Asphera, Inc.), directly coated with a 2 μm Ce polycrystalline film and overcoated with a 0.5-μm protective Al layer. The Al layer is necessary to preserve the pristine Ce material. Details of the coating procedures are available from the authors. We measured the ambient surface emissivity of the Ce–LiF interface versus wavelength for each target and found that it is consistent with prior work [28] for high-purity Ce: approximately 0.6 at 400 nm and dropping monotonically to around 0.3 at 2000 nm. The films may have a small amount of porosity, up to 10% based on prior coating experience. A porous sample assumes a higher initial shock compression temperature than a fully dense sample, but this should have no impact on the melt boundary temperatures measured during cooling of the liquid-phase shock-compressed film.

Figure 1 shows a schematic of the experiments. A planar Al or Cu impactor, accelerated to a velocity between 2.05 and 2.51 km s^{-1} by a single-stage, 40-mm bore powder gun drove a shock through the Al layer, the Ce layer, and into the LiF. The impactor diameter of 25 mm and coated window diameter of 38 mm delayed the release of stress at the window circumference, avoiding contamination of target radiance by LiF fracture luminescence while maintaining continuous uniaxial strain at the measurement radii. We measured the interface velocity near the center of the Ce–LiF interface using photon Doppler velocimetry (PDV) [29]. To determine temperature, we measured the dynamic reflectance and emitted spectral radiance of the shocked surface of the Ce, down to its optical skin depth, using previously published methods [18,19,30].

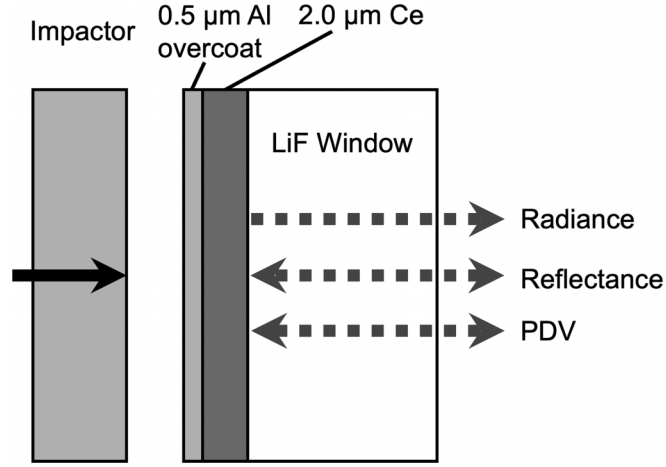

FIG. 1. A schematic of the experimental configuration. The impactor strikes the coated LiF window, and the radiance and interface velocity of the Ce–LiF interface are recorded at a common radius (4 mm) from the center, while reflectance is measured near the center.

We've made available a summary of the method and the raw data for each experiment, see Supplemental Material [31].

Figure 2 shows the temperature and interface stress measured in experiment 3. Shock impedance at these stresses is similar in LiF, Ce, and Al. Differences in initial stress between the layers were modest and equilibrated to a steady state determined by the impedance match between the LiF and impactor in a time too short to resolve. PDV measurements confirmed $\geqslant$400 ns duration of steady interface loading, ending with arrival of the release wave from the back surface of the impactor. The measured interface velocity allowed calculation of the equilibrium stress state from the stress-particle velocity relationship of LiF [32,33]. The calculated initial shock temperatures of the impactor and LiF layer are less than ~700 K, much lower than the shocked Ce film. After initial shock heating, the Ce undergoes rapid cooling as heat diffuses into the surrounding layers. The cooling is punctuated by a clear interruption caused by the temporary competition of heat conduction out of the Ce with the released heat of

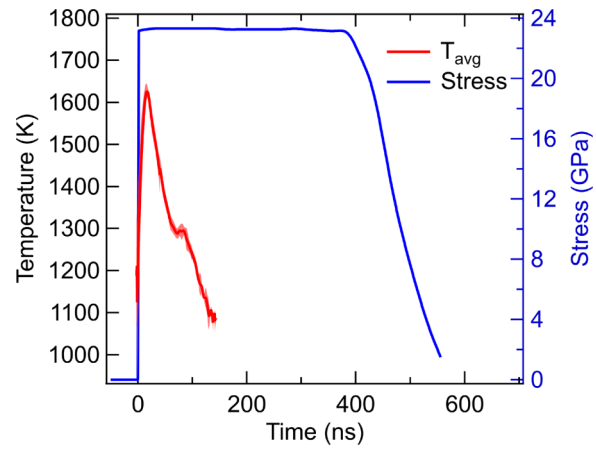

FIG. 2. Temperature (red, left axis) and stress (blue, right axis) vs time, measured at the Ce–LiF interface, for experiment 3. The resolidification signature is visible at ~75 ns and 1300 K.

TABLE I. Experimental parameters and results.

Experiment	Impactor material	Impactor velocity (m s^{-1})	Equilibrium interface stress (GPa)	Melt T (K)
1 (211209)	Al	2040	18.15	1184 ± 28
2 (220706)	Al	2378	21.96	1324 ± 32
3 (210827)	Al	2511	23.32	1295 ± 17
4 (220707)	Al	2566	24.65	1375 ± 45
5 (211214)	Cu	2046	26.93	1375 ± 44

solidification from the phase transformation. After a short time, cooling resumes, eventually dropping the temperature below the dynamic measurement limit of the pyrometer. The experimental parameters and results for all experiments are summarized in Table I. Cooling curves are shown in Fig. 3.

Figure 4 plots the observed temperature of transformation from the liquid to the ϵ phase at each measured equilibrium stress on the Ce phase diagram. These points constrain the Ce high–P liquid–ϵ phase boundary from 18 to 27 GPa. Although the timescale of our experiments is orders of magnitude shorter, we find agreement with the results of Sitaud *et al.*, acquired in a DAC [34]. Sitaud looked for a pause in temperature increase as a micron-scale sample melted under laser heating at static pressure, while we measured a pause in conductive cooling as a micron-scale sample solidified in a shock experiment. We find this agreement interesting, as static and dynamic melt boundary measurements often disagree, sometimes dramatically [11].

The duration of the interruption, prior to resumption of cooling, is roughly the time required to complete the resolidification transformation. In experiments 1, 3, and 4, the time for solidification appears to be between 25 and 50 ($\pm$10) ns. Experiment 2 shows a slower cooling curve and longer resolidification plateau of $\sim$90 $\pm$ 20 ns for unclear reasons. We speculate that either the film was thicker than expected or had a lower thermal conductivity. We observed that the LiF

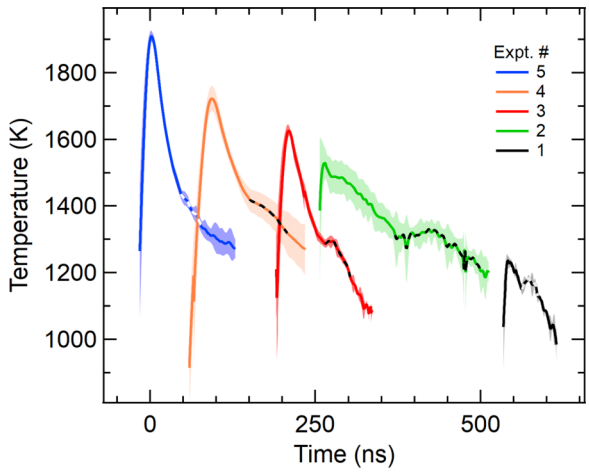

FIG. 3. Measured temperature vs time traces for each experiment, staggered in reverse order (5-1) for clarity. Resolidification temperatures in Table I are taken as the peak (1,2,3) or midpoint (4,5) of the dashed regions, with error bars chosen to span these regions.

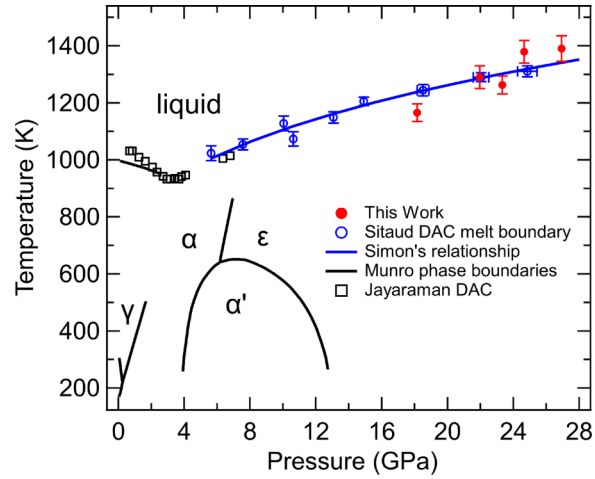

FIG. 4. The cerium phase diagram showing solid and liquid phases. The melt values reported by DAC measurements (Sitaud and Jayaraman), with a Simon's relationship curve fit, are shown in blue. Our dynamic data (red) are consistent with the static data.

sample—the only sample with this issue—was slightly hazy prior to coating, which may have caused some difference or contamination in the film. In experiment 5 the change in the cooling rate is less apparent. Its faster cooling could outcompete the outflow of latent heat and more rapidly exhaust the total amount, steepening the slope and shortening the duration of the cooling interruption. Variation of the thermal properties of the system at this higher temperature and pressure could also impart some slope to $T(t)$ through resolidification. This was also the only experiment that used a copper impactor (to achieve a higher stress). In all cases, the apparent time to complete phase transformation is considerably shorter than the melt duration time of at least 600 ns suggested by Hixson and La Lone under isobaric conditions [18]. The completion of all observed solidifications in $<$100 ns, combined with solidification times decreasing with increasing cooling rate to as little as 25 ns, suggests that any liquid-to-ϵ transition kinetics possesses characteristic timescales $<$25 ns. This suggests that target surface imperfections, such as Ce compounds formed by machining the sample or subsequent oxide/hydride growth, might be responsible for the changes in emissivity observed by Hixson and La Lone, while melt occurred rapidly.

We can use the temperature data to directly estimate the latent heat of fusion ΔH_f and transition entropy ΔS_f by comparing the measured cooling curve with the estimated cooling curve in the absence of the transition. The latter is determined by interpolation of the smoothly and slowly varying logarithmic cooling function. The integrated difference between these two curves is the ratio of the enthalpy to the specific heat capacity: $\frac{\Delta H_f}{C_p} = \frac{T\Delta S_f}{C_p}$. This ratio is similar for each experiment, roughly 164 $\pm$ 26 K. Uncertainties in this estimate include that in absolute temperature, in the beginning and end times of solidification, and the interpolation of anticipated cooling during the duration of solidification, and measurement noise.

Using $C_p \sim 0.27$ J g^{-1} K^{-1} as reported [35,36] for liquid Ce at ambient pressure, the heat of fusion, estimated from all five experiments, is $\sim$44 $\pm$ 8 J g^{-1}, and $\Delta S_f \sim 0.035 \pm 0.012$ J g^{-1} K^{-1} at experimental stresses of 18–27 GPa.

Prior to these experiments it was thought that the high-pressure enthalpy of fusion was much higher than we estimate. Elkin *et al.* [25] capture the behavior in the γ–α region of the phase diagram by treating the two phases as a pseudobinary solid solution; however, recent results appear to show that the Elkin ϵ phase boundaries [37,38] and shock Hugoniot [11,18,38] are inaccurate. In particular, the Elkin EOS significantly overpredicts the extent of the solid-liquid mixed-phase region on the Hugoniot, with $\Delta S_f = 0.192$ J g^{-1} K^{-1} at incipient melt, nearly a factor of 5 larger than we found. Using the Simon fit to the melt boundary from Sitaud *et al.*, this would correspond to $\Delta H_f = 0.192$ J g^{-1} K^{-1} $\times$ 1120 K $= 214$ J g^{-1}, an overestimate by the same factor.

We can also estimate ΔH_f and ΔS_f by fixing the Hugoniot stress values for incipient melt and melt completion to 10.2 and 13.0 GPa, respectively, based on XRD data [11]. We then determine density using recently published solid and liquid shock velocity–particle velocity fits [17]. Volume changes across the melt transition are calculated assuming an isentropic path from 10.2 $\rightarrow$ 11.6 GPa in the solid and 13.0 $\rightarrow$ 11.6 GPa in the liquid. We then apply two Birch's law fits to solid and liquid bulk sound speed data [11] and determine the enthalpy in the solid and liquid at the midpoint stress of 11.6 GPa. This gives $\Delta H_f \sim 39 \pm 20$ J g^{-1}. Dividing by the melt temperature at 11.6 GPa, we calculate $\Delta S_f \sim 0.034 \pm 0.019$ J g^{-1} K^{-1}. The given uncertainties result from uncertainties in stress at the beginning and completion of solidification, absolute temperature, and uncertainty in the P-T slope of the isentropic paths. These estimates for ΔH_f and ΔS_f based on available experimental XRD phase measurements support the values inferred from the temperature hold during resolidification. Together these data and analyses explain why the pressure range over which the mixed phase coincides with the shock Hugoniot is so narrow.

To investigate the nature of thermal diffusion in our experiments, we created one-dimensional (1D) thermal diffusion simulations, similar to those described in previous work [21,39]. We found that the initial shock temperature (T_0) of the layers translated the calculated $T(t)$ curves along the T axis. Varying the relative thermal conductivity (κ) of the layers substantially affected cooling rate, while varying heat capacity and initial temperature did not. No changes in these parameters had strong correlation to changes in enthalpy. To estimate ΔH_f from the simulation, initial shock T values were taken from simulations performed with the hydrodynamics code CTH [40]. We applied literature estimates for C_p and varied κ for each layer to produce a best fit to the observed temperature decay curves before and after resolidification, with $\Delta H_f = 0$. We then varied ΔH_f to match the experimental duration of the pause in cooling. Figure 5 shows several example $T(t)$ traces, calculated at the Ce–LiF temperature measurement interface, overlaid on the experimental data from experiment 3. Parameter values for LiF were $\kappa = 2$ W m^{-1} K^{-1}, $T_0 = 520$ K, for Ce $\kappa = 50$ W m^{-1} K^{-1}, $T_0 = 1850$ K, and for Al $\kappa = 240$ W m^{-1} K^{-1}, $T_0 = 580$ K. Uncertainty in ΔH_f is simply estimated as the values at which the calculated cooling curve diverged from the data by a factor outside of the measurement noise. The best-fit estimate for experiment 3 suggests $\Delta H_f \sim 39 \pm 6$ J g^{-1}.

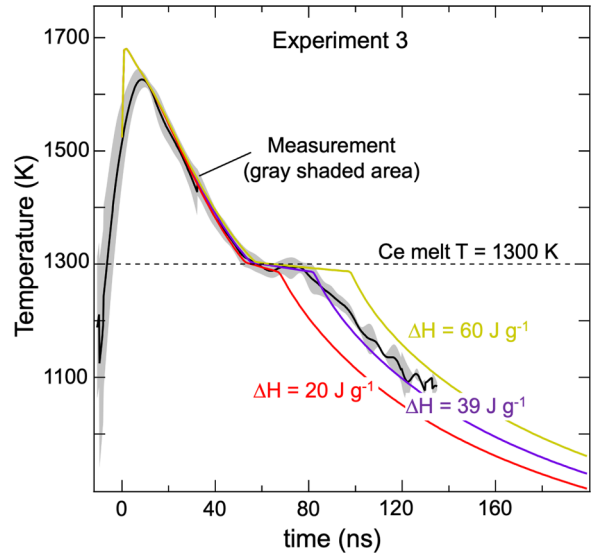

FIG. 5. Simple thermal diffusion models of experiment 3. Parameters are fit before transformation with $\Delta H_f = 0$, then ΔH_f is varied to match the model (red, purple, gold) to the data (black with gray uncertainty).

In conclusion, we have shown that thermal equilibration between thin films and bulk materials can be used to probe a range of thermal states under steady stress conditions and expose the liquid –ϵ melt boundary in Ce. The measured thermal trajectories constrain the latent heat, entropy, and heat capacity at the experimental stress and temperature. The calculated enthalpy and entropy of fusion are significantly lower than those used in the EOS model of Elkin *et al.*, explaining the narrow coexistence of the mixed-phase region and the shock Hugoniot apparent in recent experiments. The data bound the timescale of the transformation, ruling out kinetics on certain timescales. Using proper thin-film configurations, it should be possible to heat and cool various materials along isobaric paths to observe the temperature, enthalpy, and kinetics of liquid-solid and other phase transformations under dynamic compression.

We thank Lynn Veeser for valuable discussions and suggestions regarding the work and this manuscript. We also thank Ruben Valencia and Matthew Staska for their assistance in target fabrication, experimental assembly, and facility operations. Nevada National Security Sites is managed and operated by Mission Support and Test Services, LLC, under Contract No. DE-NA0003624. Los Alamos National Laboratory is operated by Triad National Security LLC for the National Nuclear Security Administration of the U.S. Department of Energy under Contract No. 89233218CNA000001.

[1] P. Bridgman, *Collected Experimental Papers* (Harvard University Press, Cambridge, MA, 2013), Vol. II, pp. 624–692.
[2] A. Jayaraman, Rev. Mod. Phys. **55**, 65 (1983).
[3] D. Bancroft, E. L. Peterson, and S. Minshall, J. Appl. Phys. **27**, 291 (1956).
[4] L. Al'tshuler, Sov. Phys. Usp. **8**, 52 (1965).
[5] J. Asay and D. Hayes, J. Appl. Phys. **46**, 4789 (1975).
[6] G. Duvall and R. Graham, Rev. Mod. Phys. **49**, 523 (1977).
[7] R. Hixson, D. Boness, J. Shaner, and J. Moriarty, Phys. Rev. Lett. **62**, 637 (1989).
[8] R. McQueen, J. Hopson, and J. Fritz, Rev. Sci. Instrum. **53**, 245 (1982).
[9] S. Tracy, S. Turneaure, and T. Duffy, Phys. Rev. Lett. **120**, 135702 (2018).
[10] R. Briggs, F. Coppari, M. Gorman, R. Smith, S. Tracy, A. Coleman, A. Fernandez-Pañella, M. Millot, J. Eggert, and D. Fratanduono, Phys. Rev. Lett. **123**, 045701 (2019).
[11] M. Beason, B. Jensen, and B. Branch, J. Appl. Phys. **128**, 165107 (2020).
[12] S. Sharma and Y. Gupta, Phys. Rev. B **104**, 064113 (2021).
[13] S. Kormer, M. Sinitsyn, G. Kirillov, and V. Urlin, Sov. Phys. JETP **21**, 689 (1965).
[14] G. Lyzenga and T. Ahrens, Geophys. Res. Lett. **7**, 141 (1980).
[15] C. Yoo, N. Holmes, M. Ross, D. Webb, and C. Pike, Phys. Rev. Lett. **70**, 3931 (1993).
[16] D. Partouche-Sebban, D. Holtkamp, J. Pélissier, J. Taboury, and A. Rouyer, Shock Waves **11**, 385 (2002).
[17] B. Jensen, T. Hartsfield, D. Holtkamp, F. Cherne, R. Corrow, T. Graves, and A. Iverson, Phys. Rev. B **102**, 214105 (2020).
[18] R. Hixson, B. La Lone, M. Staska, G. Stevens, W. Turley, and L. Veeser, J. Appl. Phys. **129**, 155106 (2021).
[19] B. La Lone, P. Asimow, O. Fat'yanov, R. Hixson, G. Stevens, W. Turley, and L. Veeser, J. Appl. Phys. **126**, 225103 (2019).
[20] T. Hartsfield and D. Dolan, J. Appl. Phys. **131**, 185901 (2022).
[21] T. Hartsfield, B. La Lone, G. Stevens, L. Veeser, and D. Dolan, J. Appl. Phys. **128**, 015903 (2020).
[22] R. Grover and P. Urtiew, J. Appl. Phys. **45**, 146 (1974).
[23] A. Jayaraman, Phys. Rev. **137**, A179 (1965).
[24] O. Tsiok and L. Khvostantsev, J. Exp. Theor. Phys. **93**, 1245 (2001).
[25] V. Elkin, V. Mikhaylov, A. Petrovtsev, and F. Cherne, Phys. Rev. B **84**, 094120 (2011).
[26] B. Jensen, F. Cherne, and N. Velisavljevic, J. Appl. Phys. **127**, 095901 (2020).
[27] A volume decrease in the Ce due to solidification would send a small rarefaction into the LiF.
[28] L. Akashev, N. Popov, and V. Shevchenko, J. Appl. Spectrosc. **85**, 624 (2018).
[29] O. Strand, D. Goosman, C. Martinez, T. Whitworth, and W. Kuhlow, Rev. Sci. Instrum. **77**, 083108 (2006).
[30] B. La Lone, G. Stevens, W. Turley, D. Holtkamp, A. Iverson, R. Hixson, and L. Veeser, J. Appl. Phys. **114**, 063506 (2013).
[31] See Supplemental Material at http://link.aps.org/supplemental/10.1103/PhysRevB.108.L140101 for a description of the methods used to measure radiance, measure reflectance, and calculate temperature, as well as the raw data from each experiment.
[32] S. Marsh, *LASL Shock Hugoniot Data* (University of California Press, Berkeley, CA, 1980).
[33] P. Rigg, M. Knudson, R. Scharff, and R. Hixson, J. Appl. Phys. **116**, 033515 (2014).
[34] B. Sitaud, J. Péré, and T. Thévenin, Int. J. High Press. Res. **12**, 175 (1994).
[35] F. Spedding, J. McKeown, and A. Daane, J. Phys. Chem. **64**, 289 (1960).
[36] I. Savchenko, D. Samoshkin, and S. Stankus, J. Eng. Thermophys. **29**, 42 (2020).
[37] K. Munro, D. Daisenberger, S. MacLeod, S. McGuire, I. Loa, C. Popescu, P. Botella, D. Errandonea, and M. I. McMahon, J. Phys.: Condens. Matter **32**, 335401 (2020).
[38] M. Beason and B. Jensen, Phys. Rev. B **105**, 214107 (2022).
[39] B. La Lone, G. Capelle, G. Stevens, W. Turley, and L. Veeser, Rev. Sci. Instrum. **85**, 073903 (2014).
[40] J. McGlaun, S. Thompson, and M. Elrick, Int. J. Impact Eng. **10**, 351 (1990).